Supplementary Information

cis-[(η^5-C_5H_5)Fe(η^1-CO)(μ-CO)]$_2$, the poor relative between *cis* and *trans* tautomers. A theoretical study of the Fe L_3-edge and C and O K-edge XAS of *trans*-/*cis*-[(η^5-C_5H_5)Fe(η^1-CO)(μ-CO)]$_2$.

Silvia Carlotto, [a,b,*] Girolamo Casella,[c] Mauro Sambi,[a,d] Maurizio Casarin[a,b,*]

[a]Dipartimento di Scienze Chimiche, Università degli Studi di Padova, Via Francesco Marzolo 1, 35131 Padova - Italy

[b]Institute of Condensed Matter Chemistry and Technologies for Energy (ICMATE), National Research Council (CNR), c/o Department of Chemistry, University of Padova, via Francesco Marzolo 1, 35131 Padova - Italy

[c]Dipartimento di Scienze della Terra e del Mare, Università degli Studi di Palermo, Via Archirafi, 22, 90123 Palermo – Italy

[d]Consorzio INSTM, Unità di Ricerca di Padova, Via Francesco Marzolo 1, 35131 Padova - Italy

Figure S1. Licorice representation of the *cis*-**I** (left) and *trans*-**I** (right) structures optimized in ref. 13 superimposed to the SR ZORA BLYP D3(BJ) ones, obtained by assuming a C_1 symmetry point group. Structure are all optimized in *vacuum* by adopting TZ2P[13] and TZ2P ZORA basis sets for all the atoms in NR and SR calculations, respectively.

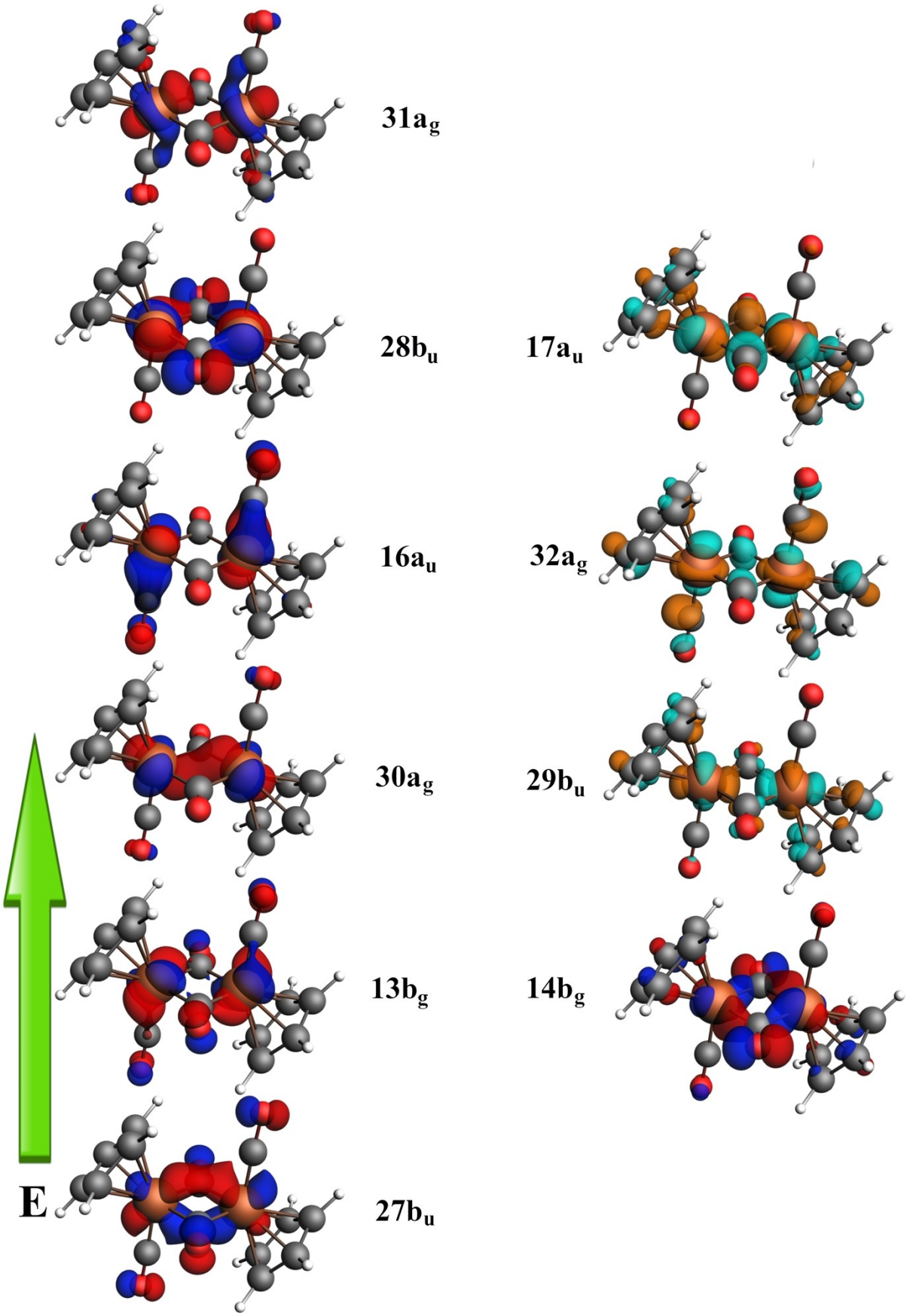

Figure S2a. 3D Plot of the *trans*-**I** t_{2g}-like (left panel) and e_g (right panel) MOs. Displayed iso-surfaces correspond to ±0.05 $e^{1/2} \times Å^{-3/2}$ values; the $14b_g$ and $29b_u$ orbitals are the HOMO and LUMO, respectively.

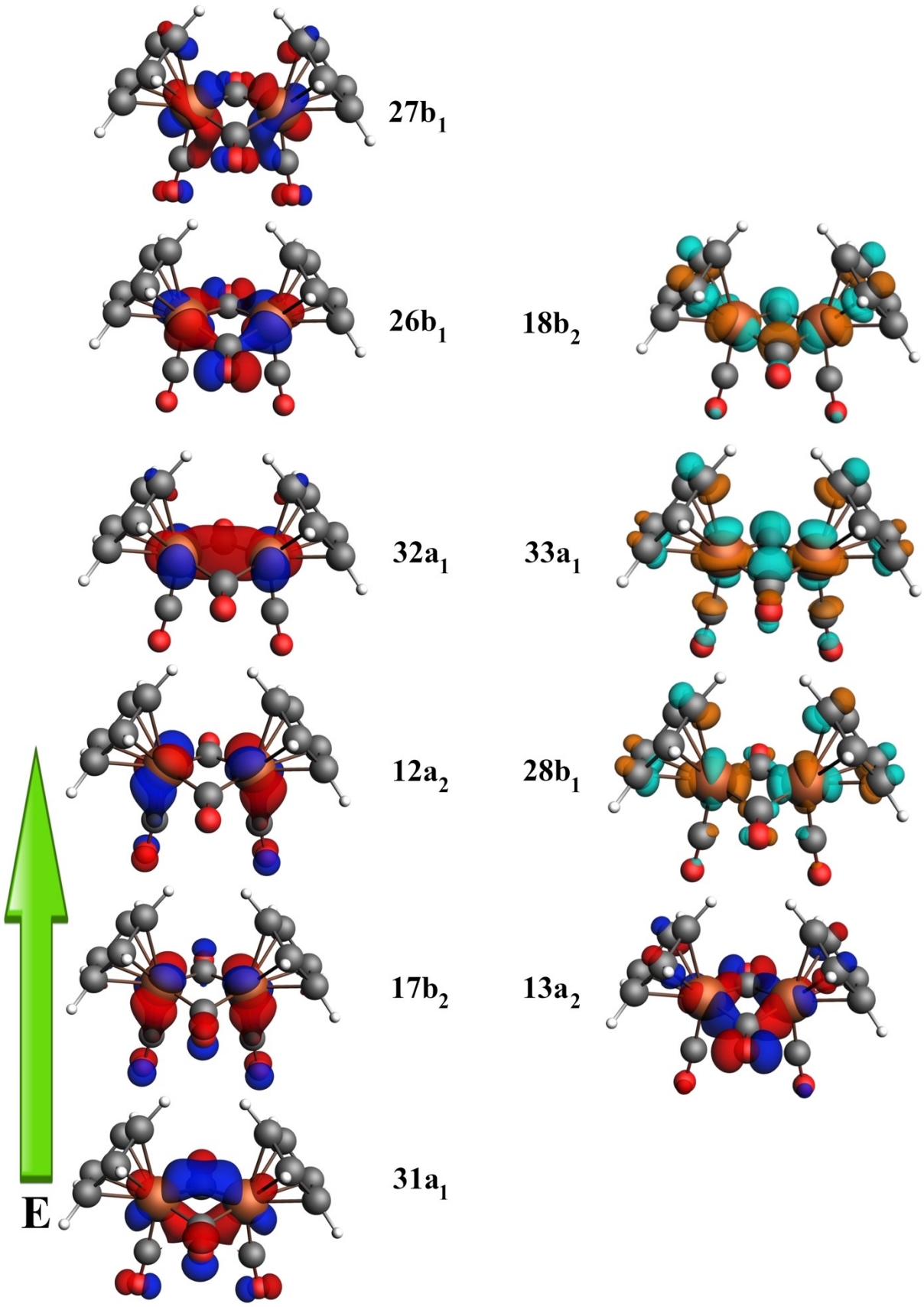

Figure S2b. 3D Plot of the *cis*-**I** t_{2g}-like (left panel) and e_g (right panel) MOs. Displayed iso-surfaces correspond to ±0.05 $e^{1/2} \times Å^{-3/2}$ values; the $13a_2$ and $28b_1$ orbitals are the HOMO and LUMO, respectively.

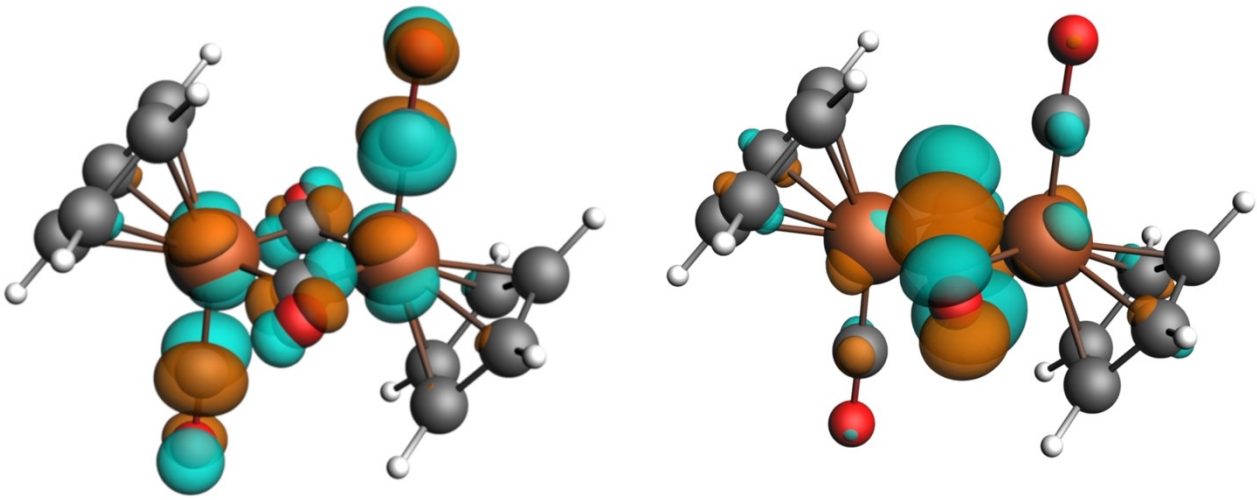

Figure S3. 3D Plot of the *trans*-**I** $15b_g$ and $16b_g$ VMOs. Displayed iso-surfaces correspond to ±0.05 $e^{1/2} \times Å^{-3/2}$ values.

Table S1. SR ZORA BLYP D3(BJ) C_1 thermodynamic quantities associated to the *trans*-**I** ⇌ *cis*-**I** equilibrium at different T.*

	cis-**I**$^{298.15}$	*trans*-**I**$^{298.15}$	*cis*-**I**^{368}	*trans*-**I**^{368}	*cis*-**I**^{383}	*trans*-**I**^{383}
Electronic Energy	-4522.25	-45232.61	-4522.25	-45232.61	-4522.25	-45232.61
Dispersion Energy	-63.11	-63.32	-63.11	-63.32	-63.11	-63.32
Total Bonding Energy (BE)	-4585.36	-4586.93	-4585.36	-4586.93	-4585.36	-4586.93
NIE†	137.21	137.24	142.82	142.84	141.86	141.87
H = (BE + NIE) **	-4448.15	-4449.69	-4442.54	-4444.09	-4443.50	-4445.06
S	143.61	144.56	160.91	161.81	164.50	165.39
TS	42.82	43.10	59.22	59.55	63.00	63.34
G = H – TS	-4490.97	-4492.79	-4501.76	-4503.64	-4506.50	-4508.40
ΔG (cis-trans)	1.82		1.88		1.90	
K_{eq}=[cis]/[trans]	0.046		0.077		0.083	

*BE, NIE, TS, H, G, ΔG in kcal × mol^{-1}; S in cal × mol^{-1} × K^{-1}; †NIE stands for Nuclear Internal Energy. **The RT contribution term has been neglected for each isomer, being the molar work term contribution calculated as: Δn × RT, with Δn = 0.

Table S2. Optimized SR ZORA BLYP D3(BJ) C_1 Cartesian coordinated of *cis*-**I**

Fe	1.270588	-0.043514	-0.020240
Fe	-1.272275	0.044402	-0.020215
C	0.039168	1.438859	-0.197717
O	0.091529	2.621935	-0.278322
O	-0.098598	-2.615255	-0.328546
C	-0.042044	-1.434123	-0.225123
C	-1.596984	0.053788	-1.746460
O	-1.870567	0.063271	-2.875587
C	1.600311	-0.021003	-1.745568
O	1.878735	-0.009665	-2.873472
C	-2.556737	1.289897	1.217686
C	-1.735776	0.486859	2.065815
C	-2.027835	-0.890990	1.802587
C	-3.011117	-0.948671	0.779769
C	-3.328738	0.407910	0.408427
H	-2.548642	2.369676	1.155731
H	-1.015854	0.859971	2.781206
H	-1.554019	-1.743915	2.269796
H	-3.426100	-1.844837	0.338611
H	-4.039853	0.704314	-0.351934
C	3.297878	-0.537118	0.423567
C	3.077737	0.860319	0.717594
C	2.104543	0.932720	1.747789
C	1.714413	-0.402998	2.087410
C	2.470622	-1.310613	1.283415
H	0.978137	-0.681544	2.828465
H	1.696849	1.842758	2.166972
H	2.384403	-2.388723	1.283046
H	3.980592	-0.926235	-0.320860
H	3.555805	1.697479	0.226696

Table S3. Optimized SR ZORA BLYP D3(BJ) C_1 Cartesian coordinated of *trans*-**I**

Fe	0.828030	-0.965962	-0.000274
Fe	-0.827961	0.965927	-0.000331
C	0.000182	0.000016	-1.446735
O	0.000264	0.000118	-2.633325
C	-0.000120	-0.000046	1.445927
O	-0.000141	-0.000096	2.632531
C	2.249474	0.052222	-0.001356
O	3.207587	0.715647	-0.001817
C	-2.249500	-0.052143	-0.001889
O	-3.207747	-0.715357	-0.002743
C	-1.996403	2.748042	0.001630
C	0.193576	2.773357	0.715906
C	0.193122	2.774581	-0.714014
C	-1.159397	2.765718	1.164014
C	-1.160055	2.767773	-1.161329
H	-3.078726	2.729116	0.001941
H	1.071270	2.754405	-1.345565
H	1.072047	2.752060	1.346959
H	-1.493387	2.738959	-2.189887
H	-1.492036	2.734757	2.192722
C	1.996359	-2.748207	0.000752
C	-0.193062	-2.773243	0.716796
C	-0.193757	-2.774588	-0.713154
C	1.160235	-2.765847	1.163836
C	1.159095	-2.767855	-1.161495
H	3.078684	-2.729347	0.000233
H	1.493683	-2.735131	2.192288
H	1.491603	-2.738984	-2.190331
H	-1.072319	-2.754372	-1.344110
H	-1.071046	-2.751824	1.348498

Table S4. SO ZORA RTD-DFT compositions (superscript in parentheses), $f \times 10^3$ and *EE* values (eV) of transitions of symmetry a_1, b_1 and b_2, associated to states generating the Fe L_3-edge in *cis*-**I** (C_{2v}).[a,b,c]

Peak	Energy (eV)	Sym.	$f \times 10^3$	Transitions[d,e,f,g,h]
L_3^1	703.2	a_1	5.6	$8e_{1/2} \rightarrow 90e_{1/2}^{(57)} + 7e_{1/2} \rightarrow 90e_{1/2}^{(20)}$
L_3^1	703.3	b_1	7.1	$8e_{1/2} \rightarrow 90e_{1/2}^{(43)} + 7e_{1/2} \rightarrow 90e_{1/2}^{(26)}$
L_3^1	703.9	b_1	12.4	$8e_{1/2} \rightarrow 91e_{1/2}^{(46)} + 10e_{1/2} \rightarrow 92e_{1/2}^{(17)} + 7e_{1/2} \rightarrow 91e_{1/2}^{(14)}$
L_3^2	704.1	a_1	10.3	$9e_{1/2} \rightarrow 92e_{1/2}^{(27)} + 7e_{1/2} \rightarrow 91e_{1/2}^{(23)} + 10e_{1/2} \rightarrow 94e_{1/2}^{(12)}$
L_3^2	704.1	b_1	10.2	$10e_{1/2} \rightarrow 92e_{1/2}^{(27)} + 8e_{1/2} \rightarrow 91e_{1/2}^{(23)} + 9e_{1/2} \rightarrow 94e_{1/2}^{(12)}$
L_3^2	704.1	b_2	11.5	$7e_{1/2} \rightarrow 92e_{1/2}^{(47)} + 8e_{1/2} \rightarrow 92e_{1/2}^{(37)}$
L_3^2	704.6	b_1	10.9	$10e_{1/2} \rightarrow 95e_{1/2}^{(44)} + 8e_{1/2} \rightarrow 93e_{1/2}^{(26)}$
L_3^2	704.7	b_1	5.6	$7e_{1/2} \rightarrow 95e_{1/2}^{(22)} + 9e_{1/2} \rightarrow 94e_{1/2}^{(14)}$
L_3^2	704.7	a_1	9.2	$8e_{1/2} \rightarrow 95e_{1/2}^{(22)} + 10e_{1/2} \rightarrow 94e_{1/2}^{(14)}$
L_3^2	704.7	a_1	5.1	$8e_{1/2} \rightarrow 95e_{1/2}^{(46)} + 7e_{1/2} \rightarrow 95e_{1/2}^{(17)} + 9e_{1/2} \rightarrow 96e_{1/2}^{(12)}$
L_3^2	704.9	a_1	10.7	$10e_{1/2} \rightarrow 97e_{1/2}^{(37)} + 7e_{1/2} \rightarrow 96e_{1/2}^{(16)} + 9e_{1/2} \rightarrow 96e_{1/2}^{(15)}$
L_3^2	704.9	b_2	13.1	$7e_{1/2} \rightarrow 95e_{1/2}^{(25)} + 10e_{1/2} \rightarrow 96e_{1/2}^{(17)} + 8e_{1/2} \rightarrow 94e_{1/2}^{(16)} + 10e_{1/2} \rightarrow 98e_{1/2}^{(14)} + 8e_{1/2} \rightarrow 95e_{1/2}^{(11)}$
L_3^2	705.2	a_1	19.8	$8e_{1/2} \rightarrow 97e_{1/2}^{(42)} + 7e_{1/2} \rightarrow 96e_{1/2}^{(10)}$
L_3^2	705.2	a_1	10.8	$7e_{1/2} \rightarrow 97e_{1/2}^{(27)} + 8e_{1/2} \rightarrow 98e_{1/2}^{(18)} + 7e_{1/2} \rightarrow 98e_{1/2}^{(14)} + 7e_{1/2} \rightarrow 96e_{1/2}^{(11)}$
L_3^2	705.2	b_1	11.2	$7e_{1/2} \rightarrow 97e_{1/2}^{(42)} + 8e_{1/2} \rightarrow 96e_{1/2}^{(10)}$
L_3^2	705.3	b_1	9.0	$8e_{1/2} \rightarrow 98e_{1/2}^{(40)} + 7e_{1/2} \rightarrow 98e_{1/2}^{(21)} + 8e_{1/2} \rightarrow 97e_{1/2}^{(12)}$
L_3^3	705.9	b_1	7.8	$9e_{1/2} \rightarrow 102e_{1/2}^{(29)} + 7e_{1/2} \rightarrow 100e_{1/2}^{(12)} + 9e_{1/2} \rightarrow 103e_{1/2}^{(12)}$
L_3^3	706.0	b_1	16.9	$7e_{1/2} \rightarrow 99e_{1/2}^{(42)} + 7e_{1/2} \rightarrow 102e_{1/2}^{(15)} + 9e_{1/2} \rightarrow 102e_{1/2}^{(13)}$
L_3^3	706.0	a_1	6.7	$8e_{1/2} \rightarrow 99e_{1/2}^{(42)} + 8e_{1/2} \rightarrow 102e_{1/2}^{(15)} + 10e_{1/2} \rightarrow 102e_{1/2}^{(13)}$
L_3^3	706.1	a_1	11.4	$8e_{1/2} \rightarrow 104e_{1/2}^{(20)} + 7e_{1/2} \rightarrow 104e_{1/2}^{(13)} + 8e_{1/2} \rightarrow 99e_{1/2}^{(13)} + 8e_{1/2} \rightarrow 100e_{1/2}^{(12)}$
L_3^3	706.1	b_1	9.3	$7e_{1/2} \rightarrow 104e_{1/2}^{(20)} + 8e_{1/2} \rightarrow 104e_{1/2}^{(13)} + 7e_{1/2} \rightarrow 99e_{1/2}^{(13)} + 7e_{1/2} \rightarrow 100e_{1/2}^{(12)}$
L_3^3	706.2	b_1	5.1	$8e_{1/2} \rightarrow 104e_{1/2}^{(69)} + 7e_{1/2} \rightarrow 104e_{1/2}^{(26)}$
L_3^3	706.3	a_1	25.9	$8e_{1/2} \rightarrow 104e_{1/2}^{(48)} + 7e_{1/2} \rightarrow 104e_{1/2}^{(15)} + 8e_{1/2} \rightarrow 99e_{1/2}^{(10)}$
L_3^3	706.3	b_1	6.5	$7e_{1/2} \rightarrow 104e_{1/2}^{(49)} + 8e_{1/2} \rightarrow 104e_{1/2}^{(15)} + 7e_{1/2} \rightarrow 99e_{1/2}^{(10)}$
L_3^3	706.3	b_2	63.6	$7e_{1/2} \rightarrow 102e_{1/2}^{(22)} + 10e_{1/2} \rightarrow 104e_{1/2}^{(21)}$

[a]The Fe *f*(*EE*) distribution displayed in the left panel of Figure 4 has been blue-shifted by 4.66 eV to allow the matching between the most intense theoretical and experimental features. [b]Contributions to iso $\rightarrow$ fso of less than 10% are not reported; [c]($f \times 10^3$) values of less than 5 are not reported. [d]Fe 2p-based levels are: $5e_{1/2}/6e_{1/2}$, $7e_{1/2}/8e_{1/2}$ and $9e_{1/2}/10e_{1/2}$ at 724.27; 711.80, and 711.57 eV, respectively. [e]The parenthood of the Fe 2p-based levels with SR ZORA Fe 2p-based MOS is: $5e_{1/2} \rightarrow 3a_1^{(33)} + 4b_1^{(32)} + 1b_2^{(31)}$; $6e_{1/2} \rightarrow 3b_1^{(33)} + 4a_1^{(32)} + 1a_2^{(31)}$; $7e_{1/2} \rightarrow 3a_1^{(56)} + 4b_1^{(33)} + 3b_1^{(5)}$; $8e_{1/2} \rightarrow 3b_1^{(56)} + 4a_1^{(33)} + 3a_1^{(5)}$; $9e_{1/2} \rightarrow 1b_2^{(59)} + 4b_1^{(30)} + 3a_1^{(5)} + 1a_2^{(5)}$; $10e_{1/2} \rightarrow 1a_2^{(59)} + 4a_1^{(30)} + 3b_1^{(5)} + 1b_2^{(5)}$. [f]The lowest unoccupied spinor is the $90e_{1/2}$. [g]The parenthood of the lowest unoccupied spinor with the SR ZORA LUMOs is $90e_{1/2} \rightarrow 28b_1^{(100)}$. [h]The parenthood of the $91e_{1/2}$, $92e_{1/2}$, $93e_{1/2}$, $94e_{1/2}$, $95e_{1/2}$, $96e_{1/2}$, $97e_{1/2}$, $98e_{1/2}$, $99e_{1/2}$, $100e_{1/2}$, $102e_{1/2}$, $103e_{1/2}$, $104e_{1/2}$ spinors with SR ZORA VMOs is $91e_{1/2} \rightarrow 33a_1^{(98)}$; $92e_{1/2} \rightarrow 18b_2^{(98)}$; $93e_{1/2} \rightarrow 34a_1^{(99)}$; $94e_{1/2} \rightarrow 14a_2^{(99)}$; $95e_{1/2} \rightarrow 19b_2^{(100)}$; $96e_{1/2} \rightarrow 29b_1^{(96)} + 35a_1^{(3)}$; $97e_{1/2} \rightarrow 35a_1^{(97)} + 29b_1^{(3)}$; $98e_{1/2} \rightarrow 20b_2^{(100)}$; $99e_{1/2} \rightarrow 30b_1^{(100)}$; $100e_{1/2} \rightarrow 36a_1^{(87)} + 21b_2^{(10)} + 15a_2^{(3)}$; $102e_{1/2} \rightarrow 15a_2^{(97)} + 36a_1^{(3)}$; $103e_{1/2} \rightarrow 16a_2^{(100)}$; $104e_{1/2} \rightarrow 31b_1^{(100)}$.

Table S5. Energy order of C and O 1s-based SALCs (σSALCs) of *cis*-**I**

	a_1	a_2	b_1	b_2
O(η^1-CO)	5		5	
O(μ-CO)	6			2
C(η^1-CO)	7		6	
C(μ-CO)	8			3
C(η^5-C_5H_5)	9+10+11	2+3	7+8+9	4+5

Table S6. SR ZORA RTD-DFT compositions (in parentheses), $f \times 10^2$ and *EE* values (eV) of transitions of symmetry a_1, b_1 and b_2, associated to states generating the C K-edge in *cis*-**I** (C_{2v}).[a,b,c,d,e]

Peak	*EE* (eV)	Sym.	$f \times 10^2$	Transitions
A	276.3	b_1	1.6	$11a_1 \rightarrow 28b_1^{(75)} + 9b_1 \rightarrow 33a_1^{(15)}$
A	276.3	a_1	2.0	$9b_1 \rightarrow 28b_1^{(75)} + 11a_1 \rightarrow 33a_1^{(15)}$
B	276.9	b_1	4.5	$3a_2 \rightarrow 18b_2^{(73)} + 5b_2 \rightarrow 14a_2^{(13)}$
B	276.9	a_1	4.0	$5b_2 \rightarrow 18b_2^{(74)} + 3a_2 \rightarrow 14a_2^{(13)}$
C	277.6	b_1	12.1	$6b_1 \rightarrow 34a_1^{(49)} + 7a_1 \rightarrow 29b_1^{(27)}$
C	277.7	a_1	3.7	$9b_1 \rightarrow 32b_1^{(16)} + 11a_1 \rightarrow 36a_1^{(12)} + 11a_1 \rightarrow 33a_1^{(12)} + 5b_2 \rightarrow 18b_2^{(11)} +$ $11a_1 \rightarrow 37a_1^{(11)} + 11a_1 \rightarrow 38a_1^{(10)}$
C	277.7	b_1	5.7	$11a_1 \rightarrow 32b_1^{(15)} + 9b_1 \rightarrow 36a_1^{(12)} + 9b_1 \rightarrow 33a_1^{(12)} + 9b_1 \rightarrow 37a_1^{(11)} +$ $3a_2 \rightarrow 18b_2^{(11)} + 9b_1 \rightarrow 34a_1^{(10)} + 9b_1 \rightarrow 38a_1^{(10)}$
C	277.9	b_2	10.9	$6b_1 \rightarrow 14a_2^{(36)} + 7a_1 \rightarrow 19b_2^{(18)} + 7a_1 \rightarrow 20b_2^{(15)} + 7a_1 \rightarrow 18b_2^{(14)}$
C	278.4	b_1	1.8	$5b_2 \rightarrow 15a_2^{(30)} + 3a_2 \rightarrow 21b_2^{(17)} + 3a_2 \rightarrow 22b_2^{(16)} + 5b_2 \rightarrow 14a_2^{(11)}$ $3a_2 \rightarrow 18b_2^{(10)} + 9b_1 \rightarrow 34a_1^{(10)} + 9b_1 \rightarrow 38a_1^{(10)}$
C	278.7	a_1	5.3	$3b_2 \rightarrow 19b_2^{(73)} + 3b_2 \rightarrow 20b_2^{(23)}$

[a]*EE*s herein reported have been evaluated by adopting the PBE0 XC functional. [b]The C *f*(*EE*) distribution displayed in the left, upper panel of Figure 6 has been blue-shifted by 9.80 eV to allow the matching between the most intense theoretical and experimental features. [c]Contributions to iso $\rightarrow$ fso of less than 10% are not included; [d]($f \times 10^2$) values of less than 1.5 are not included. [e]The C 1s-based SALCs lye at: -281.55 eV ($7a_1 + 6b_1$; η^1-CO); -281.13 eV ($8a_1 + 3b_2$; μ-CO); -279.54 eV ($9a_1 + 7b_1$; η^5-C_5H_5); -279.52 eV ($2a_2 + 4b_2$; η^5-C_5H_5); -279.50 eV ($8b_1 + 10a_1$; η^5-C_5H_5); -279.49 eV ($3a_2 + 5b_2$; η^5-C_5H_5); -279.48 ($9b_1 + 11a_1$; η^5-C_5H_5).

Table S7. SR ZORA TD-DFT % compositions (in parentheses), $f \times 10^3$ and *EE* values (eV) of transitions of symmetry a_1, b_1 and b_2 associated to states generating the O K-edge of *cis*-**I** (C_{2v}).[a,b,c,d,e]

Peak	*EE* (eV)	Sym.	$f \times 10^3$	Transitions
S	529.2	a_1	7.2	$2b_2 \rightarrow 19b_2^{(84)} + 6a_1 \rightarrow 35a_1^{(14)}$
S′	529.5	a_1	11.8	$6a_1 \rightarrow 35a_1^{(56)} + 2b_2 \rightarrow 20b_2^{(38)} + 2b_2 \rightarrow 19b_2^{(5)}$
S′	529.7	a_1	28.6	$2b_2 \rightarrow 20b_2^{(61)} + 6a_1 \rightarrow 35a_1^{(30)} + 2b_2 \rightarrow 19b_2^{(8)}$
S′	529.9	b_1	9.2	$5b_1 \rightarrow 34a_1^{(93)}$
S′	530.0	b_2	9.3	$5b_1 \rightarrow 14a_2^{(76)} + 5a_1 \rightarrow 19b_2^{(19)}$
A	530.5	b_1	22.7	$2b_2 \rightarrow 15a_2^{(78)} + 6a_1 \rightarrow 30b_1^{(20)}$
A	530.6	b_1	31.7	$5a_1 \rightarrow 29b_1^{(87)}$
A	530.6	b_2	21.7	$5a_1 \rightarrow 20b_2^{(92)}$
B	531.1	b_1	6.3	$2b_2 \rightarrow 16a_2^{(98)}$
B	531.3	b_2	16.6	$5b_1 \rightarrow 15a_2^{(95)}$

[a]*EE*s herein reported have been evaluated by adopting the LB94 XC functional. [d]The O *f*(*EE*) distribution displayed in the right, upper panel of Figures 6 has been blue-shifted by 3.57 eV to allow the matching between the most intense theoretical and experimental features. [b]Contributions to iso → fso of less than 10% are not included; [c]($f \times 10^3$) values of less than 5 are not included. [e]The O 1s-based SALCs lye at: -538.08 eV ($5b_1 + 5a_1$; η^1-CO); -537.23 eV ($6a_1 + 2b_2$; μ-CO).